

**Improved reproducibility for myocardial ASL
Impact of physiological and acquisition parameters**

Božić-Iven, Maša; Rapacchi, Stanislas; Tao, Qian; Pierce, Iain; Thornton, George; Nitsche, Christian; Treibel, Thomas A.; Schad, Lothar R.; Weingärtner, Sebastian

DOI

[10.1002/mrm.29834](https://doi.org/10.1002/mrm.29834)

Publication date

2023

Document Version

Final published version

Published in

Magnetic Resonance in Medicine

Citation (APA)

Božić-Iven, M., Rapacchi, S., Tao, Q., Pierce, I., Thornton, G., Nitsche, C., Treibel, T. A., Schad, L. R., & Weingärtner, S. (2023). Improved reproducibility for myocardial ASL: Impact of physiological and acquisition parameters. *Magnetic Resonance in Medicine*, 91(1), 118-132. <https://doi.org/10.1002/mrm.29834>

Important note

To cite this publication, please use the final published version (if applicable).
Please check the document version above.



Copyright

Other than for strictly personal use, it is not permitted to download, forward or distribute the text or part of it, without the consent of the author(s) and/or copyright holder(s), unless the work is under an open content license such as Creative Commons.

Takedown policy

Please contact us and provide details if you believe this document breaches copyrights.
We will remove access to the work immediately and investigate your claim.

Improved reproducibility for myocardial ASL: Impact of physiological and acquisition parameters

Maša Božić-Iven^{1,2}  | Stanislas Rapacchi³  | Qian Tao²  | Iain Pierce⁴  | George Thornton^{4,5}  | Christian Nitsche^{4,5,6}  | Thomas A. Treibel^{4,5}  | Lothar R. Schad¹ | Sebastian Weingärtner² 

¹Medical Faculty Mannheim, Heidelberg University, Mannheim, Germany

²Department of Imaging Physics, Delft University of Technology, Delft, The Netherlands

³CNRS, CRMBM, Aix-Marseille Université, Marseille, France

⁴Barts Heart Centre, St Bartholomew's Hospital, London, UK

⁵Institute of Cardiovascular Science, University College London, London, UK

⁶Division of Cardiology, Medical University of Vienna, Vienna, Austria

Correspondence

Sebastian Weingärtner, Department of Imaging Physics, Delft University of Technology, Lorentzweg 1, 2628CJ Delft, The Netherlands.

Email: S.Weingartner@tudelft.nl

Funding information

4TU federation; BHF Clinical Research Training Fellowship, Grant/Award Number: FS/CRTF/21/24127; British Heart Foundation Intermediate Fellowships, Grant/Award Number: FS/19/35/34374; Landesgraduiertenförderung Baden-Württemberg; NWO Start-up grant, Grant/Award Number: STU.019.024; ZonMW Off-Road, Grant/Award Number: 04510011910073

Abstract

Purpose: To investigate and mitigate the influence of physiological and acquisition-related parameters on myocardial blood flow (MBF) measurements obtained with myocardial Arterial Spin Labeling (myoASL).

Methods: A Flow-sensitive Alternating Inversion Recovery (FAIR) myoASL sequence with bSSFP and spoiled GRE (spGRE) readout is investigated for MBF quantification. Bloch-equation simulations and phantom experiments were performed to evaluate how variations in acquisition flip angle (FA), acquisition matrix size (AMS), heart rate (HR) and blood $T_{1,B}$ relaxation time ($T_{1,B}$) affect quantification of myoASL-MBF. In vivo myoASL-images were acquired in nine healthy subjects. A corrected MBF quantification approach was proposed based on subject-specific $T_{1,B}$ values and, for spGRE imaging, subtracting an additional saturation-prepared baseline from the original baseline signal.

Results: Simulated and phantom experiments showed a strong dependence on AMS and FA ($R^2 > 0.73$), which was eliminated in simulations and alleviated in phantom experiments using the proposed saturation-baseline correction in spGRE. Only a very mild HR dependence ($R^2 > 0.59$) was observed which was reduced when calculating MBF with individual $T_{1,B}$. For corrected spGRE, in vivo mean global spGRE-MBF ranged from 0.54 to 2.59 mL/g/min and was in agreement with previously reported values. Compared to uncorrected spGRE, the intra-subject variability within a measurement (0.60 mL/g/min), between measurements (0.45 mL/g/min), as well as the inter-subject variability (1.29 mL/g/min) were improved by up to 40% and were comparable with conventional bSSFP.

Conclusion: Our results show that physiological and acquisition-related factors can lead to spurious changes in myoASL-MBF if not accounted for. Using individual $T_{1,B}$ and a saturation-baseline can reduce these variations in spGRE and improve reproducibility of FAIR-myASL against acquisition parameters.

KEYWORDS

cardiac arterial spin labeling, cardiac magnetic resonance imaging, flow-sensitive alternating inversion recovery, myocardial blood flow

1 | INTRODUCTION

First-pass myocardial perfusion with cardiac MR (CMR) is widely used as the clinical gold standard for noninvasive assessment of myocardial ischemia.¹⁻⁴ However, the need for exogenous, gadolinium-based contrast agents, limits the clinical applicability of first-pass perfusion MRI. Since gadolinium is cleared from the body almost exclusively through the kidneys,^{5,6} gadolinium-based contrast agents are contraindicated in patients with renal dysfunction.⁶ Additionally, concerns have been raised about gadolinium accumulation in the brain following the repeated use of gadolinium-based contrast agents, even in combination with healthy renal clearance.^{7,8}

Arterial Spin Labeling (ASL) offers a contrast-agent free alternative for perfusion measurements, using magnetically labeled blood as an endogenous contrast.^{9,10} ASL has been well established in neuro-vascular applications and has steadily gained importance in quantifying cerebral blood flow over the last decades.^{11,12} In cardiac applications, promising results have been achieved with myocardial ASL (myoASL): Reported myoASL-based myocardial blood flow (MBF) values were in agreement with reference values from positron emission tomography (PET) gold standard measurements.¹³ Moreover, myoASL has shown to be sensitive to perfusion changes induced by either vasodilatory stress or when comparing normal and ischemic myocardial segments.¹⁴ However, due to a low signal-to-noise ratio, insufficient reproducibility and robustness have hampered more wide-spread clinical translation of myoASL thus far.¹⁵

Typically, multiple pairs of tag and control images are acquired in an ASL measurement. In tag images magnetically labeled blood is flowing into the imaging volume, while no labeling is applied for control images. Subtracting tag from control yields perfusion weighted images, which can then be used to quantify the MBF.^{13,16,17} With signal differences between tag and control images of 1%–8%,¹⁸ myoASL is rendered very sensitive to physiological signal variations, such as those caused by cardiac or respiratory motion. This physiological noise (PN) was found to be the

dominant noise source in myoASL.¹³ However, its ratio to thermal noise is highly dependent on the choice of imaging readout and acquisition parameters.¹⁹ In myoASL, the perfusion weighted signal is most commonly acquired using snapshot image readouts, where all k-space lines are acquired in a single heartbeat. To obtain quantitative MBF, however, the perfusion weighted signal is modeled only based on the effects of the labeling preparation.¹⁶ As the imaging pulses perturb the magnetization signal, the image contrast can still be dependent on parameters related to image readout. This can cause a number of factors, including sequence parameters such as the acquisition flip angle or physiological parameters such as the heart rate variability, to affect the precision and bias of ASL measurements.

The objective of this study is to investigate the effect of physiological and acquisition-related parameters on the bias and precision of quantitative myoASL measurements. Simulation and phantom experiments are used to evaluate the relative contribution of various confounders in balanced steady-state free precession (bSSFP) and spoiled gradient-echo (spGRE) based myoASL. Next, we propose an improved MBF calculation approach to alleviate some of those confounders, to reduce the bias, and, potentially in extension, help to improve the reproducibility of Flow-sensitive Alternating Inversion Recovery (FAIR) myoASL. Namely, subject-specific blood T_1 relaxation times and, for spGRE readouts only, additional saturation-prepared baseline acquisitions are used to calculate MBF. Finally, the repeatability of myoASL with and without corrections is studied in healthy volunteers.

2 | THEORY

2.1 | ASL signal model

MBF quantification in myoASL is most commonly based on Buxton's general kinetic model (GKM).¹⁶ In the GKM, the difference between control and tag signal is modeled based on the transport of inverted magnetization into the imaging volume with arterial blood. The present work

focuses on a FAIR-ASL sequence (Figure 1), for which the GKM can be derived as:

$$MBF = \frac{\lambda(I_C - I_T)}{\delta I_{BL} T I e^{-TI/T_{1,B}}}, \quad (1)$$

with control (I_C), tag (I_T), and baseline signal (I_{BL}), inversion time TI, inversion efficiency $\delta = 1 - \cos(\alpha_{inv})$, blood-water partition coefficient $\lambda = 1 \text{ mL/g}$,^{20,21} and blood T_1 relaxation time $T_{1,B}$. Due to the substantially faster flow in the heart compared to other anatomies, the labeling slab is considered to be small relative to the fast flow in coronary arteries during the TI.¹⁷ Therefore, as previously applied in cardiac ASL,^{17,22} in the present work it has been decided to neglect the effect of the ATT in the model as a first approximation.

2.2 | Magnetization modulation function

Imaging in myoASL has been previously proposed with bSSFP or spGRE snapshot readouts. These readouts lead

to a significant modulation of the magnetization, which is expressed as a magnetization modulation function (MMF, f_{MMF}) throughout this work.

The signal equations for bSSFP and spGRE readout are provided in Appendix A. They can be simplified in the form of a general affine linear model for the MMF:

$$f_{MMF}(x) = Ax + B. \quad (2)$$

Here, the coefficients A and B depend on the acquisition parameters as well as T_1 and T_2 , while $x = M_z(t_0)$ represents the initial magnetization immediately prior to the readout. Due to the low systolic coronary blood flow,^{23,24} in- and out-flow effects during the image readout were considered negligible and, thus, were not explicitly considered in the MMF. Based on the MMFs in the Appendix (Equations (A1), (A5)), A and B are given as

$$A = \begin{cases} \sin\left(\frac{\alpha}{2}\right) \left(E_1 \cos^2\left(\frac{\alpha}{2}\right) + E_2 \sin^2\left(\frac{\alpha}{2}\right)\right)^n, & \text{bSSFP} \\ \rho \cos^n(\alpha) E_1^{n-1}, & \text{spGRE} \end{cases} \quad (3)$$

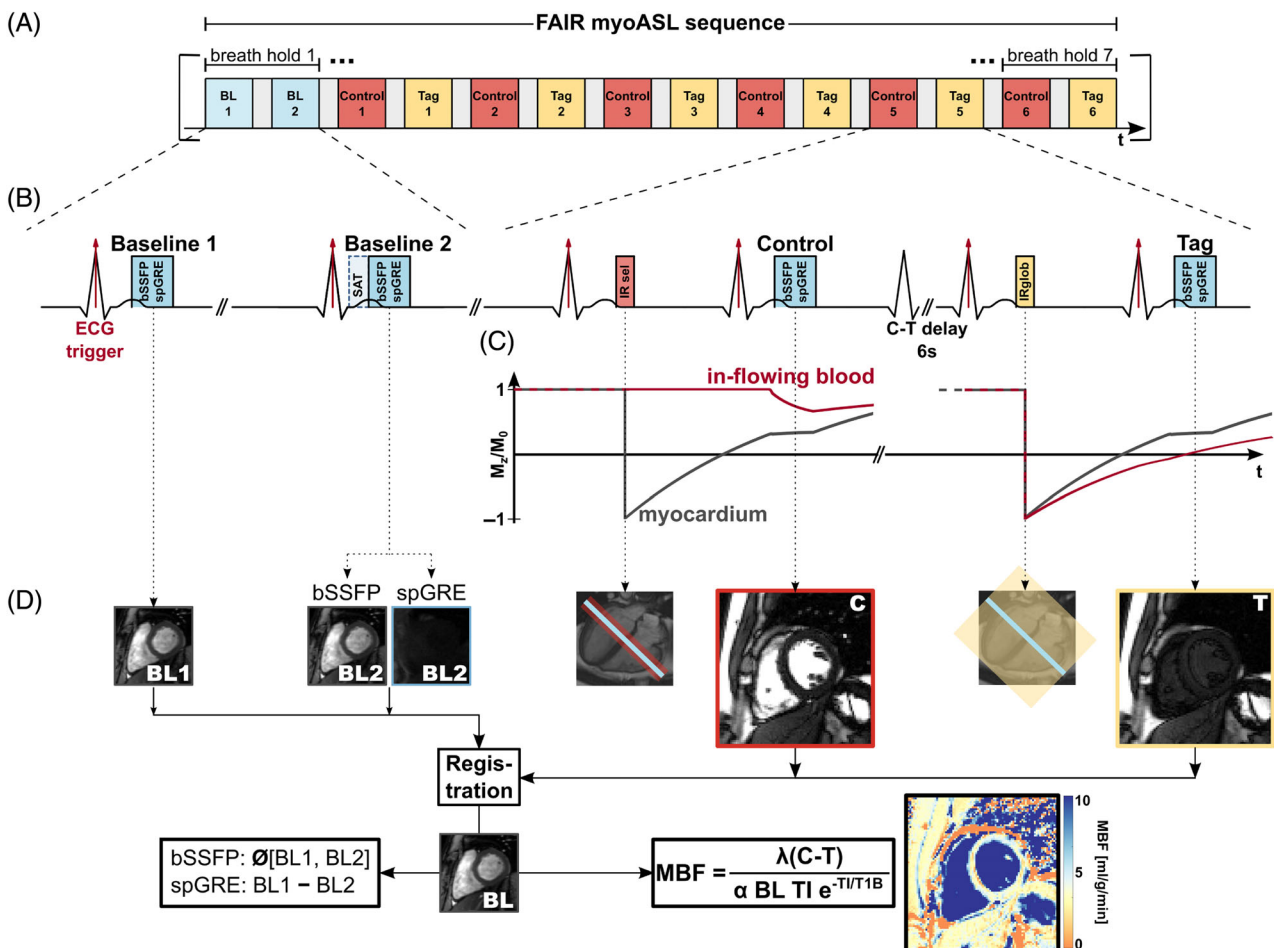


FIGURE 1 (A, B) Sequence diagram of the FAIR-myocardial ASL sequence and (D) processing pipeline used in this study. (C) Temporal evolution of the longitudinal magnetization after an initial inversion pulse and during the imaging readout in the subsequent heartbeat.

and

$$B = \begin{cases} \left(1 - \left(E_1 \cos^2\left(\frac{\alpha}{2}\right) + E_2 \sin^2\left(\frac{\alpha}{2}\right)\right)^n\right) M_{ss}, & \text{bSSFP} \\ \frac{1 - \cos(\alpha) E_1^{n-1}}{1 - \cos(\alpha) E_1} (1 - E_1) \cos(\alpha) \rho M_{z,eq}, & \text{spGRE} \end{cases} \quad (4)$$

with $E_{1/2} = e^{-TR/T_{1/2}}$, proton density ρ , steady-state and equilibrium longitudinal magnetization M_{ss} and $M_{z,eq}$, flip angle (FA) α , and n applied imaging pulses.

2.2.1 | FAIR-myASL sequence

In a FAIR-myASL measurement, the imaging signal can be modeled with blood (I_B) and myocardial contributions (I_M) weighted by the blood-volume-fraction V_B and its complement $V_M = 1 - V_B$, respectively. Due to differences in the relaxation times,^{25,26} the coefficients A_M and A_B in the MMF (Equations 3 and 4) differ between I_B and I_M .

Using the approach of Buxton's GKM (Equation 1) and the image signals as derived in the Appendix (Equations B2–B9), the ratio of control, tag, and baseline signal can be given as:

$$\frac{I_C - I_T}{I_{BL}} = \frac{V_B f_{in} A_B (x_B^+ - x_B^-)}{V_M (A_M x_M^+ + B_M) + V_B (A_B x_B^+ + B_B)}. \quad (5)$$

This relation only yields the unbiased, true perfusion rate f_{in} , in the case of $A_B = A_M = 1$ and $B_B = B_M = 0$ which is implicitly assumed in Buxton's GKM. In an experimental setting, however, this condition is not met due to the long echo trains ($n \gg 1$) in particular for snapshot readouts. Hence, the obtained perfusion rate is confounded by acquisition parameters such as the FA and the acquisition matrix size (AMS), which determines the number of imaging pulses applied prior to the k-space center.

These acquisition parameters can, thus, influence the precision and accuracy of the measurement. Figure 2 illustrates the interdependencies for a selection of parameters relevant to this study, namely: AMS, acquisition FA, heart rate variations, $T_{1,B}$, and blood flow. Most of these factors, such as the FA and AMS, affect the accuracy and might impart bias on FAIR-myASL-based MBF. However, because these parameters might vary on different time scales, they can also compromise the reproducibility and even repeatability of FAIR-myASL.

2.2.2 | Saturation-baseline

As apparent from Equation (5), eliminating the coefficients B_B and B_M from the image signal can reduce the dependence on acquisition parameters. This can

	repeatability (short term)	reproducibility (long-term)	bias (systematic)
acquisition matrix size	none	high	high
flip angle (FA) prescribed FA	none	low	high
flip angle (FA) B_1^+ inhomogeneity	low	high	high
heart rate	high	high	high
blood T_1	none	low*	high
blood flow**	low	low	low

*depending on the time scale of the observation

**blood flow is the measurand and as such induces a bias profile rather than confounding the measurement

FIGURE 2 Various acquisition-related (acquisition flip angle and matrix size) and physiological parameters (heart rate, blood T_1 , blood flow) influence the precision (repeatability, reproducibility) and accuracy (bias) of FAIR-myASL measurements. Except for blood flow effects during image readout, these factors were investigated in this work. Parameters affected by the proposed correction approach are framed in red. Repeatability is mainly influenced by physiological noise, while reproducibility relates to variability on longer time scales and between systems/set-ups. Bias relates to intrinsic systematic deviations and is a common source of lack of reproducibility.³⁸ The different factors manifest as different types of myocardial blood flow (MBF) errors depending on their respective time scale: Different prescribed matrix sizes and flip angle values in separate measurements as well as subject-specific B_1^+ field distributions impart different biases and impair reproducibility.^{46,61} Further, a varying heart rate (HR) can cause changes in the coronary blood flow⁶²—a major source of physiological noise—as well as in the sequence timing, which confounds MBF values and renders them subject to different biases. Repeatability and reproducibility can further be compromised by changes in the HR across control-tag pairs or across measurements/subjects, respectively. As the value of $T_{1,B}$ depends on numerous physiological factors which might change over longer periods of time, this can affect the MBF bias and reproducibility. Finally, replacement of spins due to flow-effects can alter the magnetization modulation function in FAIR-myASL, potentially imparting bias and compromising reproducibility.

be achieved with the acquisition of an additional saturation-prepared baseline image ($I_{BL,Sat}$), such that the signal only represents the imaging readout and not the magnetization history anymore. To this end, a saturation prepulse immediately prior to the baseline image can be used. Assuming perfect saturation, the initial magnetization of both myocardium and blood can be considered to be zero ($x_M = x_B = 0$) for the saturation-baseline signal. If the signal difference between the saturation and original

baseline (see Equation B10) is used instead of the original baseline signal in Equation (5), the ratio of control and tag image becomes:

$$\begin{aligned} \frac{I_C - I_T}{I_{BL} - I_{BL,Sat}} &= \frac{V_B f_{in} A_B (x_B^+ - x_B^-)}{V_M A_M x_M^+ + V_B A_B x_B^+} = \\ &= \frac{V_B f_{in} (x_B^+ - x_B^-)}{V_M \frac{A_M}{A_B} x_M^+ + V_B x_B^+}. \end{aligned} \quad (6)$$

Due to the different MMFs, this leads to different factors $\frac{A_M}{A_B}$ in Equation (6) for the two readout types:

$$\frac{A_M}{A_B} = \begin{cases} \left(\frac{E_{1,M} \cos^2\left(\frac{\alpha}{2}\right) + E_{2,M} \sin^2\left(\frac{\alpha}{2}\right)}{E_{1,B} \cos^2\left(\frac{\alpha}{2}\right) + E_{2,B} \sin^2\left(\frac{\alpha}{2}\right)} \right)^n, & \text{bSSFP} \\ e^{-(n-1) \cdot TR \cdot \left(\frac{1}{T_{1,M}} - \frac{1}{T_{1,B}}\right)}, & \text{spGRE} \end{cases}. \quad (7)$$

Notably, the use of the saturation-baseline eliminates the FA dependence for the case of spGRE readout and the only residual acquisition parameter related influence is given by the AMS n . With bSSFP readout, however, the signal ratio remains both FA and AMS dependent as the transverse magnetization contributes to the readout signal at each TR.

3 | METHODS

3.1 | MyoASL sequence

Based on the considerations above, a double ECG-triggered FAIR-ASL sequence building on the design by Do et al. ^{22,27} is proposed. As depicted in Figure 1, nonlabeled control and labeled tag images are acquired in an alternating fashion. For the control image, a spatially selective, adiabatic inversion pulse is applied in one heartbeat. The image acquisition is performed in the subsequent heartbeat during the same cardiac phase. To ensure consistent inversion within the imaging slice, the inversion slab is chosen three times as thick as the imaging slice. Following a 6 s long delay, the tag image is acquired in the same fashion but using a non-selective adiabatic inversion pulse. Each myoASL measurement comprised six pairs of control and tag images, referred to as individual scans, using either bSSFP or spGRE readouts.

Additionally in each measurement, a pair of baseline images was acquired without preceding inversion pulses. For bSSFP readouts, both baseline images are acquired without any preparation pulses, while for spGRE an additional saturation prepulse is added immediately prior to the readout of the second baseline image.

Postprocessing of images including MBF quantification and statistical analysis was performed in MATLAB (MathWorks). The MBF was quantified using Buxton's GKM as described in Equation (1). For bSSFP-based MBF calculation, the baseline signal I_{BL} corresponds to the average of the two baseline images. With spGRE readout, the saturation-baseline image $I_{BL,Sat}$ is subtracted from the original one and the difference image is used as the baseline value in MBF calculations as given in Equation (6). As shown in Equation (7), this saturation-baseline correction does not eliminate FA dependencies in bSSFP readouts and is therefore not applied for those. The double ECG-triggering of both labeling pulses and image readouts leads to a variable, heart rate dependent TI. For MBF calculation, TI was evaluated using either individual TIs, an average inversion time \overline{TI} for each control-tag pair, or a global TI averaged per sequence.

In previous studies on cardiac ASL, $T_{1,B}$ was set to a fixed, literature based value between 1650 and 1700 ms. ^{13,22,28,29} To avoid discrepancies with the actual T_1 , subject-specific T_1 relaxation times are used in a second quantification method.

In summary, perfusion values were calculated in four different modes depending on the readout:

- bSSFP readout with conventional, uncorrected MBF calculation (fix $T_{1,B}$, no saturation-baseline)
- bSSFP readout with corrected MBF calculation (measured individual $T_{1,B}$, no saturation-baseline)
- spGRE readout with conventional, uncorrected MBF calculation (fix $T_{1,B}$, no saturation-baseline)
- spGRE readout with corrected MBF calculation (measured individual $T_{1,B}$ and saturation-baseline)

Based on previous FAIR-myoASL studies, ^{13,27,29} the uncorrected MBF calculation from bSSFP-images is considered as the reference configuration throughout the remainder of this work.

3.2 | Imaging

All imaging was performed at 3T. In all experiments, a WET saturation pulse ^{30,31} has been used for preparation of the saturation-baseline. The detailed sequence parameters for all experiments are provided in Table 1.

3.2.1 | Phantom experiments

A phantom comprising 13 NiCl₂-doped agarose vials submerged in agarose gel was used, with T_1 relaxation times ranging between 1100 and 2500 ms and T_2 relaxation times between 50 and 170 ms. For further

TABLE 1 Sequence parameters of the FAIR-myoASL sequence for phantom and in vivo measurements.

Experiment	FA (°)		TE/TR (ms)		Matrix size	FOV (mm ²)	HR (bpm)	Resolution/slice thickness	Partial Fourier/generalized auto-calibrating partially parallel acquisition rate
	bSSFP	spGRE	bSSFP	spGRE					
Phantom – Varying HR	70	15	1.6/3.3	3.3/6.3	160 × 160	280 × 280	40–120		
Phantom – Varying FA	1–80	1–40	1.6/3.3	3.3/6.3	160 × 160	280 × 280	60	1.7 × 1.7 mm ²	6/8
					208 × 208	364 × 364		8 mm	R = 2
In vivo	70	18	1.2/2.4	1.9/2.9	154 × 192	272 × 340	n/a		

Abbreviations: FA, flip angle; FOV, field of view; HR, heart rate; spGRE, spoiled GRE; TE, echo time; TR, pulse repetition time.

evaluation, five vials with relaxation times in the physiological range were selected. Phantom experiments were performed at 3T (Magnetom Skyra, Siemens Healthineers). The FAIR-myoASL sequence was used with the acquisition parameters provided in Table 1.

Three sets of experiments were performed to investigate the effect of physiological and acquisition parameters, respectively. First, phantom data were acquired for both readout types for a range of FAs in bSSFP and spGRE with two matrix sizes (i.e., with different AMS). Further, images were acquired with varying simulated HR which resulted in varying *TI* and, lastly, with fixed HR, FA and AMS for control-tag delays between 6 and 12 s.

Prior to further processing, the signal polarity had been restored based on the recovery curves obtained with different TIs.³² To simulate the effect of flow during TI, a blood volume fraction of 0.14³³ and a blood replacement/in-flow rate of 0.29 1/s were simulated, resulting in an effective MBF input value of 2.4 mL/g/min. The assumed in-flow rate corresponds to about 4 mL/s for a myocardial blood volume of 15 mL (about 10% of the left-ventricular mass^{34,35}). Following Equations (B7)–(B9), the control, tag and baseline signals were generated from the image signal of different vials, which was obtained from manually drawn ROIs. The inverted signal contributions to I_C and I_T were taken from the selective and non-selective inversion recovery, respectively. For the myocardial signal, a vial with T_1/T_2 relaxation time of 1460/45 ms was used. The blood signal was taken from four different vials with T_1 relaxation times of 1770–2300 ms and T_2 relaxation times of 45–124 ms.

In addition to the phantom experiments, numerical simulations have been performed to assess the effect of the same physiological and acquisition-related parameters on myoASL-based MBF. Details can be found in the Numerical Simulations section of the Appendix S1.

3.2.2 | In vivo experiments

The present study was approved by the local institutional review board and written informed consent was obtained from all participants prior to examination. Nine healthy subjects (3 female, 6 male, 36 ± 8 years) with no history or current symptoms of cardiovascular disease were included in this study. The in vivo scans were performed at 3T (Magnetom Prisma, Siemens Healthineers).

MOLLI³² T_1 maps were acquired in each subject to obtain blood T_1 ($T_{1,B}$) times in the corrected MBF calculation. In the individual T_1 maps, an ROI was manually drawn in the left ventricle and $T_{1,B}$ was determined as the mean value across all pixels within this ROI. For FAIR-myoASL, labeling and imaging were placed in the systole for increased perfusion signal.²⁸ The detailed imaging parameters are given in Table 1. In six out of the nine subjects, two repetitions of two FAIR-myoASL sequences (bSSFP and spGRE) were acquired. Images were acquired during 12–16 s long breath-holds, depending on the subject's heart rate, with one image pair (baseline/control-tag) per breath-hold.

Each FAIR-myoASL sequence consisted of seven breath-holds: one for the baseline images and six for the six control-tag image pairs. The bSSFP and spGRE data sets were group-wise registered for each subject.³⁶ Subsequently, control-tag pairs subject to ECG mis-triggering or a difference in TI larger than approximately 120 ms were excluded prior to image analysis. For each subject, the myocardium as well as a septal ROI were segmented manually.³⁷ Pixel-wise perfusion maps and segment-wise septal MBF were obtained using uncorrected calculation in bSSFP and spGRE as well as corrected spGRE calculation as described above. Global MBF values are reported as the mean MBF across the myocardial ROI and across all control-tag image pairs in each repetition. Mean septal

MBF values are reported as the septal MBF averaged across all control-tag image pairs.

3.2.3 | Statistical analysis

In simulation and phantom experiments, the correlation of MBF with HR and FA was assessed using Spearman's correlation, respectively. To further evaluate the HR and FA dependence, slope and intercept values were obtained from a linear regression of simulation and phantom MBF. Moreover, the relative MBF error $\left(\frac{\text{MBF}_{\text{phantom}} - \text{MBF}_{\text{true}}}{\text{MBF}_{\text{true}}}\right)$ was compared across the calculation modes using a Friedman test for group-wise comparison, followed by a Wilcoxon signed-rank test for pair-wise comparison. For in vivo septal MBF and each readout-calculation combination, the intra-subject variability within a measurement $\overline{\sigma_p}$ was calculated as the PN averaged across all subjects:

$$\overline{\sigma_p} = \frac{1}{N_S} \sum_{j=1}^{N_S} \text{PN}_j, \quad (8)$$

with number of subjects $N_S = 9$. The PN for each repetition m with $N_{CT}^{j,m}$ control-tag image pairs is obtained as¹³

$$\begin{aligned} \text{PN}_{j,m} &= \frac{1}{\sqrt{N_{CT}^{j,m}}} \sigma(\text{MBF}_{j,m})_{N_{CT}^{j,m}} \\ &= \sqrt{\frac{\sum_{i=1}^{N_{CT}^{j,m}} (\text{MBF}_{i,j,m} - \overline{\text{MBF}}_{j,m})^2}{N_{CT}^{j,m} (N_{CT}^{j,m} - 1)}}. \end{aligned} \quad (9)$$

The mean between-measurement, intra-subject variability \overline{wsSD} of each sequence was defined as the difference in mean MBF from the two repetitions scaled by $\sqrt{2}$ and averaged over the corresponding subcohort ($N_S = 6$):³⁸

$$\begin{aligned} \overline{wsSD} &= \frac{\sum_{j=1}^{N_S} wsSD_j}{N_S} \\ wsSD_j &= \frac{|\overline{\text{MBF}}_{j,1} - \overline{\text{MBF}}_{j,2}|}{\sqrt{2}}. \end{aligned} \quad (10)$$

Lastly, the inter-subject variability $isSD$ was evaluated as the SD across the individual mean MBF values:

$$\begin{aligned} isSD &= \sqrt{\frac{\sum_{j=1}^{N_S} (\overline{\text{MBF}}_j - \overline{\text{MBF}})^2}{N_S - 1}} \\ \overline{\text{MBF}} &= \frac{1}{N_S} \sum_{j=1}^{N_S} \overline{\text{MBF}}_j. \end{aligned} \quad (11)$$

In subjects with multiple repetitions, only MBF data from the first repetition has been used to obtain $\overline{\sigma_p}$

and $isSD$. The intra- and inter-subject variability were compared across the calculation modes using a Friedman test for group-wise comparison, followed by a Wilcoxon signed-rank test for pair-wise comparison. A significance level of 0.05 was used in all statistical tests.

4 | RESULTS

4.1 | Phantom results

Simulated perfusion showed negligible differences whether calculated with individual TIs, an average inversion time \overline{TI} for each control-tag pair, or a global TI averaged per sequence as shown in Figure S1. Therefore, in all further phantom and in vivo measurements MBF was calculated with a pairwise averaged \overline{TI} for each control-tag pair. While differently evaluated TIs in MBF calculation led only to small changes in the MBF deviation, the HR variability appeared as a major confounder in myoASL-MBF.

The following phantom results are shown for all four combinations of readout and MBF calculation. Here, corrected calculation in bSSFP refers to using individual $T_{1,B}$ values, but no saturation-baseline which is only applied for spGRE as explained in the Section 3. The relative error in simulated and phantom MBF for varying control-tag delays is shown in Figure S2. For uncorrected as well as corrected calculations, the MBF values from bSSFP and spGRE readouts were largely constant over the range of applied control tag delays. The difference in MBF between a 6 s long delay and the steady state was <2.2%/<6.0% (bSSFP/spGRE) in simulations and <4.8%/<3.8% (bSSFP/spGRE) in phantom experiments. Thus, a control-tag delay of 6 s was chosen for all further experiments.

4.1.1 | Flip angle

Figure 3 shows the phantom MBF plotted against the acquisition FA for two different AMSs. In uncorrected bSSFP, phantom MBF increased with increasing FA for all vials ($0.73 < R^2 < 0.86$, slope: 0.01–0.02) except one (T_1/T_2 of 1770/45 ms), where MBF was underestimated with increasing FA ($R^2 = 1$, slope: -0.004). For all vials, longer AMS resulted in increased MBF values. This FA dependence remained for bSSFP readout when MBF was calculated with $T_{1,B}$ -correction ($0.73 < R^2 < 1$). In uncorrected spGRE, MBF values correlated strongly with FA ($0.82 < R^2 < 1$). Phantom MBF decreased with increasing FA and was lower for longer AMS for all vials, with linear slopes of -0.017 to -0.027 . Using corrected

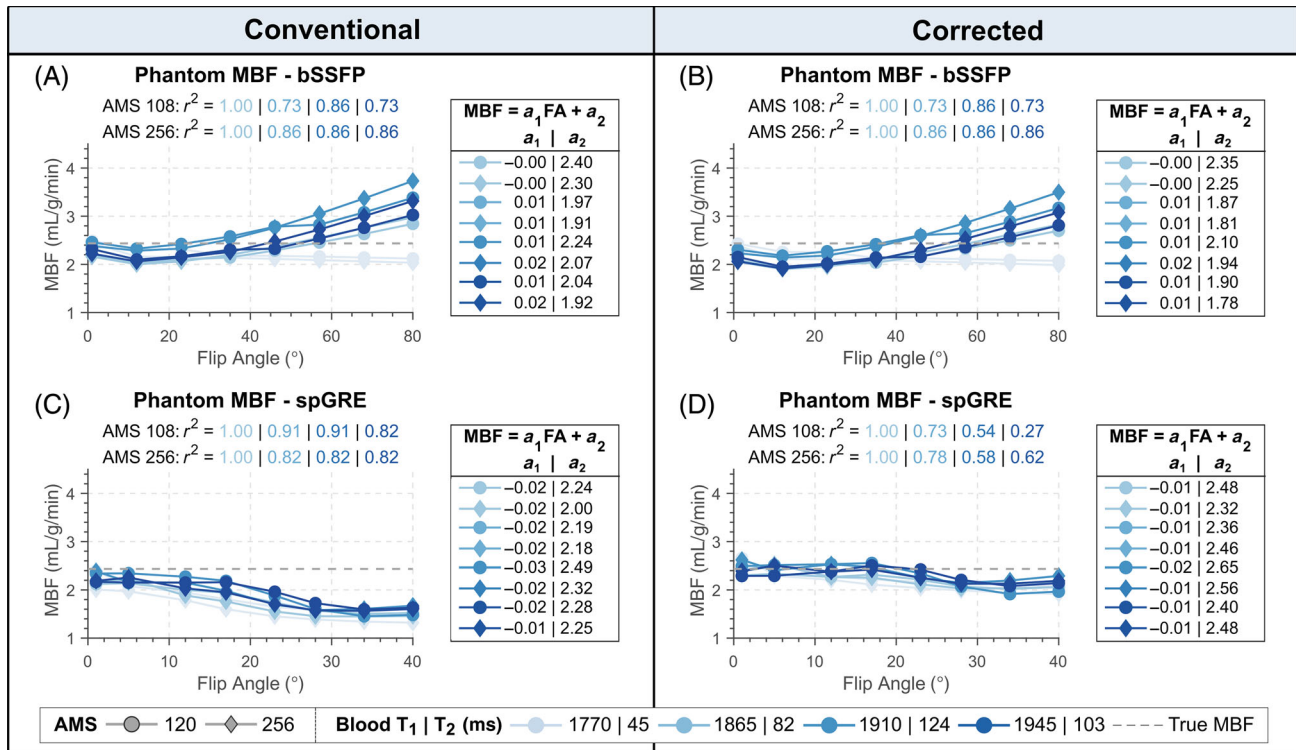


FIGURE 3 Phantom myoASL-MBF from bSSFP and spoiled GRE (spGRE) readouts. Myocardial blood flow (MBF) was calculated with (A), (C) fixed and (B), (D) individual blood T_1 ($T_{1,B}$). Additionally, for corrected spGRE (D) the saturation-baseline approach as proposed in this work was used in MBF calculation. MBF is shown as a function of acquisition flip angle (FA) for two acquisition matrix sizes (AMS) and four phantom vials (i.e. different blood T_1 and T_2). The slope (a_1) and intercept (a_2) for each vial are obtained from linear regression. Across all vials, a strong FA dependence of bSSFP- and spGRE-based MBF is observed and this effect is exacerbated for larger AMS. When the proposed correction is used in spGRE readouts, the FA dependence is alleviated over the range of acquired FAs.

calculation, spGRE-based MBF stayed largely constant around 2.48 mL/g/min up to about 25° from where it decreased slightly to 2.14 mL/g/min ($0.27 < R^2 < 1$, slope: -0.006 to -0.010). For all vials, group-wise comparison revealed a significant difference in relative MBF error among the compared readout-calculation combinations ($p < 0.05$). With fully corrected calculation in spGRE-readouts, the relative MBF error was significantly reduced compared to uncorrected spGRE ($p < 0.05$) in all vials and showed a small, non-statistically significant reduction compared to uncorrected bSSFP ($0.05 < p < 0.25$) in all vials except one ($p = 0.74/0.84$ for AMS 120/256, T_1/T_2 of 1865/82 ms). Thus, the saturation-baseline approach was used for the correction of spGRE readouts in the remainder of this work.

Phantom-based MBF values from different vials are plotted as a function of simulated HR in Figure S3. If an incorrect $T_{1,B}$ was used for quantification, phantom MBF showed a weak dependency on the HR (on average 0.01 mL/g/min per 100 ms change in RR). This effect was more pronounced with larger difference between actual and quantification $T_{1,B}$ (1700 ms). Significant

differences in relative MBF error were observed among the three readout-calculation combinations when examined through group-wise comparison ($p < 0.05$). When the correct $T_{1,B}$ was used, the relative MBF error was significantly reduced compared to uncorrected MBF calculation ($p < 0.05$) and MBF values were largely constant with HR for both readout types ($0.03 < R^2 < 0.21/0.30 < R^2 < 0.64$ bSSFP/spGRE). A bias in MBF of 0.43/0.16 mL/g/min (bSSFP/spGRE) remained across the different T_1/T_2 values.

Simulated MBF from bSSFP-readouts was overestimated with increasing FA and AMS whether calculated with or without individual $T_{1,B}$ (slope: 0.02–0.06, $R^2 = 1$), as depicted in Figure S4. For the case of uncorrected spGRE, MBF was largely constant up to FAs of about 5°, and was increasingly underestimated with FA increasing beyond 5° (slope: -0.08 to -0.07 , $R^2 = 1$). With fully corrected calculation, spGRE-based MBF was largely constant over the entire range of FAs (AMS 120: slope 0.0, $0.0 < R^2 < 0.30$; AMS 256: slope 0.0–0.01, $0.11 < R^2 < 0.44$). As shown in Figure S5, simulated spGRE-based MBF was constant over the range of simulated blood T_2 values, while bSSFP-based MBF showed a strong nonlinear relation.

MBF obtained with bSSFP and spGRE readouts showed a moderate dependence on $T_{1,B}$, which is eliminated when calculated with the correct $T_{1,B}$. Increasing measurement errors in $T_{1,B}$ led to increasing MBF errors (approximately 3% per 100 ms) for all four combinations of readout and calculation mode (Figure S6). Further, if an inaccurate $T_{1,B}$ is used in quantification, MBF shows a weak HR dependence in both readouts, as illustrated in Figure S7, which is alleviated when calculated with true $T_{1,B}$.

4.2 | In vivo results

Based on the relatively mild effect of $T_{1,B}$ compared to the FA on simulated and phantom MBF, in vivo results from bSSFP readouts are presented with uncorrected MBF calculation only. Over all subjects, mean blood $T_{1,B}$ was 1860 ± 68 ms and the HR ranged from 47 to 72 bpm. Perfusion maps and corresponding PN maps of the myocardium are shown for two representative subjects in Figure 4. For uncorrected bSSFP, mean global MBF \pm PN were 3.05 ± 0.76 mL/g/min and 0.75 ± 0.34 mL/g/min for the two subjects, respectively. In spGRE, global MBF was $3.14 \pm$

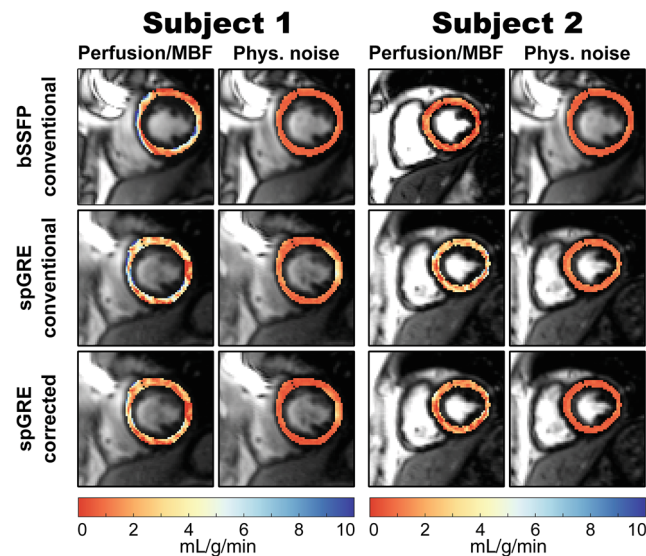


FIGURE 4 MyoASL-perfusion and physiological noise (PN) maps for two representative subjects. For uncorrected bSSFP/spGRE readouts, mean global myocardial blood flow (MBF) \pm PN was $3.05 \pm 0.76/3.14 \pm 1.52$ mL/g/min in subject 1 and $0.75 \pm 0.34/2.63 \pm 1.36$ mL/g/min in subject 2. Uncorrected bSSFP-maps appear visually more homogeneous and show lower PN across the myocardium compared to uncorrected spGRE-maps. With the proposed correction, however, spGRE-maps were on par with uncorrected bSSFP-maps showing improved image quality and reduced PN compared to uncorrected spGRE. Mean global MBF \pm PN in this case was 1.98 ± 0.96 mL/g/min in subject 1 and 1.67 ± 0.87 mL/g/min in subject 2.

$1.52/2.63 \pm 1.36$ mL/g/min (subject 1/2) with uncorrected and $1.98 \pm 0.96/1.67 \pm 0.87$ mL/g/min (subject 1/2) with fully corrected calculation. In visual assessment, uncorrected bSSFP-based maps appeared more homogeneous compared to uncorrected spGRE-based maps. With corrected MBF calculation, however, the image quality of spGRE-based perfusion maps was improved compared to the uncorrected spGRE-maps and visually comparable to the conventional bSSFP approach.

The intra-subject variability within ($\overline{\sigma_p}$) and between measurements (\overline{wsSD}) as well as the inter-subject variability (\overline{isSD}) based on septal MBF are displayed in Figure 5 for the three different combinations of readout and MBF calculation. In group-wise comparison, $\overline{\sigma_p}$ and \overline{wsSD} showed significant differences among the three combinations of readout and calculation mode ($p < 0.05$). Mean within-measurement, intra-subject variability

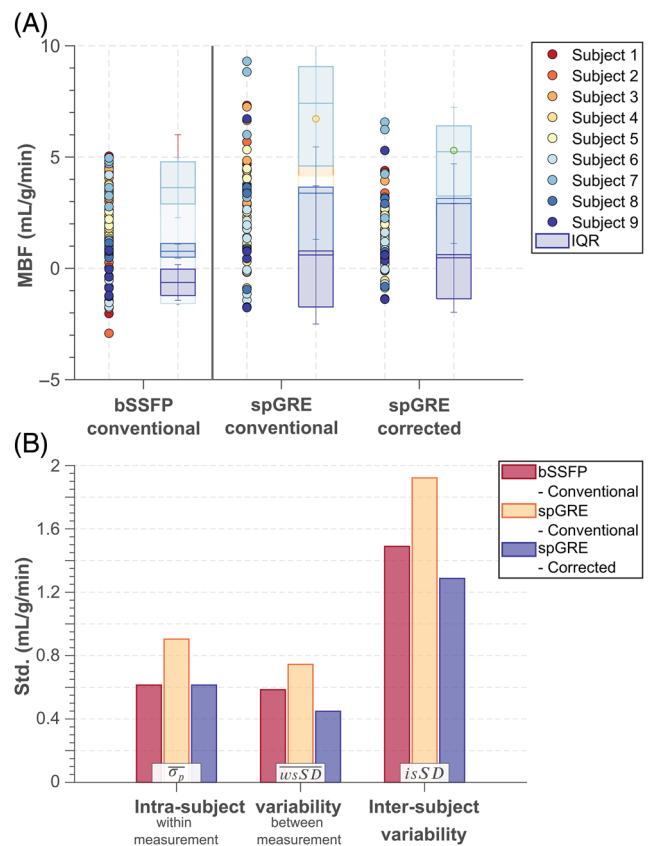


FIGURE 5 (A) In vivo septal myoASL-MBF for all acquired control-tag pairs and all nine subjects. With uncorrected calculation, myocardial blood flow (MBF) from spGRE readouts showed larger variation compared to bSSFP-based MBF. When MBF was calculated with the proposed correction, however, the spread in spGRE-MBF values was reduced compared to both uncorrected bSSFP and spGRE. This is also reflected in the (B) mean intra- and inter-subject variability: With the proposed correction, spGRE readouts show improved reproducibility compared to uncorrected spGRE and are comparable to uncorrected bSSFP.

was lower in uncorrected bSSFP (0.61 mL/g/min) than in uncorrected spGRE (0.90 mL/g/min, $p = 0.30$). The mean within-measurement, intra-subject variability in corrected spGRE-based MBF calculation (0.60 mL/g/min) was on par with uncorrected bSSFP ($p = 0.73$). Uncorrected bSSFP showed lower $wsSD$ (0.58 mL/g/min, $p = 0.44$) and $isSD$ (1.49 mL/g/min) compared to uncorrected spGRE (0.74 and 1.92 mL/g/min, respectively). However, when spGRE-MBF was calculated with individual $T_{1,B}$ and saturation-baseline, $wsSD$ was reduced compared to uncorrected spGRE by 40% ($p < 0.05$) and showed a slight but not significant reduction compared to uncorrected bSSFP 22% ($p = 1.0$). With fully corrected MBF quantification, the $isSD$ of spGRE-MBF was reduced compared to uncorrected bSSFP/spGRE by 13%/33%, respectively.

5 | DISCUSSION

In this work, we investigated how physiological and acquisition-related parameters affect FAIR-myocardial MBF measurements, when bSSFP or spGRE readouts are used. Our simulation and phantom experiments suggest that, out of the investigated parameters, the acquisition FA has the strongest effect on the MBF and may cause spurious MBF deviations. Through an adapted baseline acquisition this effect can be mitigated for spGRE readouts. Furthermore, inaccurate blood T_1 relaxation times in the MBF calculation led to a mild HR dependence which can be reduced if calculated with individual $T_{1,B}$. Using both approaches, spGRE-MBF measurements with increased reproducibility have been obtained.

This study uses the Buxton GKM which is a common choice with cardiac FAIR-ASL.^{13,17,22} However, several simplifications are made when applying this kinetic model. Importantly, the arterial transit time (ATT) effect is considered to be negligible due to the relatively small size of the labeling slab compared to the relatively fast flow in the coronary arteries. However, ATT is known to be a major confounder to accurate perfusion measurements in other anatomies,³⁹ and the validity of this simplification in cardiac applications warrants thorough investigation. Alternative approaches, such as saturation preconditioning of the signal preceding the bolus edge,⁴⁰ or velocity selective labeling,^{41,42} where labeling and imaging volumes coincide, are promising for mitigating this confounder. Furthermore, measurements, with multiple postlabeling delays may allow for joint quantification of the ATT to fully correct for this effect.⁴³ These approaches and the meteorological characterization of the impact of ATT on FAIR-based cardiac ASL quantification remain an important topic of future studies.

In this study, imaging is performed during systole, when blood flow is minimal,^{23,24} resulting in less than 1% of spins being exchanged throughout the imaging readout. Consequently, the MMF is only very weakly affected by flow and spin-exchange during the acquisition readout. However, in approaches that involve extended imaging readouts during diastole or continuous imaging readouts, like “cine-ASL”⁴⁴, the in-flow effect becomes more relevant. Recently proposed numerical models aim to capture this phenomenon,⁴⁵ offering a promising avenue for future research in cardiac ASL. Additionally, the proposed correction scheme assumes that the MMF is identical for baseline, control and tag acquisitions. While this is a common assumption in all ASL techniques,¹⁶ differences in MMF among those images may be caused by factors such as changes in the in-flow rate during the readout or changes in the effective FA. To that end, repeating baseline acquisitions throughout the measurement may be useful to minimize the resulting variability in perfusion calculation.

The acquisition FA was identified as a strong confounder in simulated and phantom myoASL-MBF measurements. In both simulation and phantom experiments, bSSFP-based MBF increased with increasing FA while spGRE-based MBF decreased with increasing FA, when conventionally calculated. As a result of the increased number in applied RF pulses, the effect of the imaging readout is exacerbated for larger AMS used in a snapshot readout. These results are especially relevant in view of the high B_1^+ variability across the myocardial region. Particularly at 3T, variations of up to 50% of the nominal FA have been observed.⁴⁶ In order to alleviate this FA dependence, we proposed an adapted baseline acquisition and MBF calculation for spGRE readouts using an additional saturation-baseline image. Due to the nature of the MMF in bSSFP, this approach can only correct for FA effects with spGRE readouts. However, in this case, the FA dependence is fully eliminated in simulated MBF and substantially reduced in phantom experiments, potentially alleviating a major acquisition-related confounder.

Perfusion values were comparable between bSSFP and spGRE readouts in simulation and phantom experiments. However, bSSFP-based MBF showed a larger variability with blood T_1/T_2 relaxation times compared to spGRE due to the T_2 dependence of the bSSFP readout signal. Our simulation and phantom results further show that a mismatch between true and quantification $T_{1,B}$ may render myoASL-MBF mildly dependent on HR. Cardiac ASL has previously been reported in the literature with intra-subject variability between 7.5%²⁷ and 28%.²⁸ In the present study, those values ranged between 26% and 39%. Thus, acquisition-related factors, such as FA and AMS, can have a relevant impact on the measurement error in cardiac ASL (up to 60% of MBF). HR-related factors, on

the other hand, were found to be mostly negligible in our results (up to 2% of MBF). As a result, the effect of using individual $T_{1,B}$ to alleviate the HR dependence is less noticeable in visual assessment compared to using the saturation-baseline for FA correction. Nonetheless, in light of the prevalence of T_1 mapping in clinical practice,⁴⁷ individual $T_{1,B}$ values can easily be obtained in common CMR examinations, and can often be incorporated without adding extra scans to the protocol.

In vivo, mean global MBF values from uncorrected bSSFP readout (2.10 ± 0.95 mL/g/min) agreed with previously reported PET-based resting MBF (0.74 – 2.43 mL/g/min⁴⁸). Compared to the reported MBF at rest in healthy subjects as obtained from first-pass perfusion MRI (0.62 ± 0.13 to 1.24 ± 0.19 mL/g/min^{49,50}), the observed myoASL-MBF values were elevated across all readout and calculation mode combinations. However, previous studies using myoASL reported values between 0.7 and 2.7 mL/g/min^{13,22,27,51} for global resting MBF. Those values are comparable to the obtained results using the bSSFP readout with uncorrected MBF calculation across all but one subject. Compared to the previously reported range for myoASL-based MBF, uncorrected spGRE-based MBF values were elevated (2.59 ± 1.37 mL/g/min). When calculated with the correction, however, spGRE-based MBF (0.54 – 2.59 mL/g/min) was generally in line with this range and comparable to uncorrected bSSFP. The lowest observed perfusion values ranged at the lower end of MBF values reported in first-pass perfusion literature (0.62 – 1.24 mL/g/min).⁵⁰

With uncorrected calculation, spGRE-based MBF showed higher PN, intra- and inter-subject variability compared to bSSFP-based MBF. This is in agreement with previous findings which demonstrate lower signal-to-noise ratio and temporal signal-to-noise ratio in cardiac imaging with spGRE snapshot imaging compared to bSSFP readout.¹⁹ Calculating spGRE-based perfusion with the proposed correction tended to improve precision: Both intra-subject variability and average PN from corrected spGRE readouts were on par with uncorrected bSSFP-based values, while simultaneously providing reduced sensitivity to FA-related effects. Similarly, the corrected spGRE approach resulted in less inter-subject variability compared to both uncorrected bSSFP and spGRE.

Nonetheless, variability in those measurements remains high. This is likely due to PN, caused by temporal fluctuations of the blood flow. Changes in the heart rate can further induce timing variations within a control-tag pair potentially impairing the variability if not accounted for. Lastly, residual motion after registration, such as caused by beat-to-beat variability or inconsistent breath-holds, might add to the uncertainty

in perfusion values. Further sequence development, such as free-breathing or motion-corrected acquisitions, and research into advanced postprocessing are warranted to address these sources of variability. With respect to diagnosis of myocardial ischemia, stress MBF cut-off values ranged between 0.91 and 1.86 mL/g/min,^{52,53} with stress MBF values in healthy volunteers of 1.97 up to 4.5 mL/g/min.⁵⁰ Thus, an effect size of about 55% can be expected. The inter-subject variability obtained in the present work, promises only moderate detection of those changes. Thus, further reduction of the variability in FAIR-myASL remains crucial for achieving diagnostic confidence as required in the clinic.

As it is common to ECG gated acquisitions, excessive heart rate variability in combination with inadequate gating windows can lead to imaging in different effective cardiac phases.⁵⁴ Thus, in double ECG-gated FAIR-myASL, this effect can lead to incongruence between the control and tag image. Due to the relatively stable duration of the systole compared to the diastole,⁵⁵ however, recent studies suggest that systolic FAIR-myASL can offer higher robustness to such timing issues.²⁸ Future studies in targeted cohorts, such as patients suffering from cardiac arrhythmia, are warranted to further investigate the suitability of systolic cardiac ASL in the clinic.

In the proposed work the correction was derived for the case of a FAIR-ASL sequence. However, the proposed saturation-baseline approach does not depend on the labeling mode and is applicable to other ASL schemes such as velocity⁴² or acceleration selective ASL.⁵⁶ In fact, Zhang et al. proposed a similar approach to account for magnetization saturation in Look-Locker FAIR-myASL (LL-FAIR)⁵⁷ using multivariate regression to eliminate the T_1 error. However, the performance was not compared to conventional fitting approaches and the proposed method was not explored in other myoASL sequences.

This study has several limitations. Current FAIR-myASL methods generally do not allow for extensive myocardial coverage since large inversion slabs can lead to increasing, nonnegligible transit delays.^{43,58} Velocity selective labeling may allow for larger myocardial coverage as it is largely insensitive to transit delays, albeit with potential sensitivity to residual motion.^{41,42} Future studies applying the proposed MBF calculation to velocity-selective ASL are warranted. The FAIR-myASL sequence was acquired in healthy subjects at rest only and no stress perfusion has been obtained. Repeatability, as assessed by back-to-back scanning, presents only a subset of the factors influencing reproducibility or intra-subject variability in a clinical setting. Further, the reproducibility and sensitivity of the corrected FAIR-myASL approach remain to be evaluated in patients with myocardial pathology. Due to the relatively small number of subjects

included in this proof-of-principle study, larger studies assessing precision in a clinical setup or reproducibility over more extended time periods or different scan settings are warranted and would also allow for increased statistical power in comparing the uncorrected and corrected MBF calculation in bSSFP and spGRE readout. In this study, individual $T_{1,B}$ were obtained with MOLLI T_1 -mapping, which is known to underestimate T_1 .^{26,59} This could lead to inaccurate $T_{1,B}$ and, as shown in the results, impair the effectiveness of the proposed MBF calculation with individual $T_{1,B}$ to reduce the HR dependence of myoASL-MBF. To that end, saturation based T_1 mapping sequences can be used in future work.⁶⁰

6 | CONCLUSION

Myocardial ASL can offer a contrast-agent free alternative for myocardial perfusion assessment. Calculating myoASL-MBF with inaccurate $T_{1,B}$ may lead to a mild heart rate dependence of MBF which was reduced by using individual $T_{1,B}$ values. Moreover, spurious MBF changes due to a varying acquisition flip angle were identified as the strongest confounder. With spGRE readouts, this effect was mitigated through the acquisition of an additional saturation-baseline image. This approach can improve the robustness of myoASL and its potential clinical use in future.



ACKNOWLEDGMENTS

The authors would also like to thank Joao L. S. C. Tourais and Scannexus Imaging Center, Maastricht, The Netherlands, for their support with preliminary phantom and in vivo measurements. This work was supported by the 4TU federation, a NWO Start-up grant STU.019.024, and ZonMW Off-Road 04510011910073. Maša Božić-Iven is funded by a PhD scholarship from the Landesgraduiertenförderung Baden-Württemberg. George Thornton is funded by a BHF Clinical Research Training Fellowship (FS/CRTF/21/24127). Thomas A. Treibel is directly and indirectly supported by the University College London Hospitals NIHR Biomedical Research Centre and Biomedical Research Unit at Barts Hospital, respectively. Thomas A. Treibel is funded by British Heart Foundation Intermediate Fellowships (FS/19/35/34374).

CONFLICT OF INTEREST STATEMENT

The authors declare no potential conflict of interests.


ORCID

Maša Božić-Iven  <https://orcid.org/0000-0003-4922-3961>
Stanislas Rapacchi  <https://orcid.org/0000-0002-8925-495X>

Qian Tao  <https://orcid.org/0000-0001-7480-0703>

Iain Pierce  <https://orcid.org/0000-0001-8546-5023>

George Thornton  <https://orcid.org/0000-0003-3289-2413>

Christian Nitsche  <https://orcid.org/0000-0002-0141-7639>

Thomas A. Treibel  <https://orcid.org/0000-0003-1560-7414>

Sebastian Weingärtner  <https://orcid.org/0000-0002-0739-6306>

REFERENCES

- Atkinson DJ, Burstein D, Edelman RR. First-pass cardiac perfusion: evaluation with ultrafast MR imaging. *Radiology*. 1990;174:757-762.
- Gerber BL, Raman SV, Nayak K, et al. Myocardial first-pass perfusion cardiovascular magnetic resonance: history, theory, and current state of the art. *J Cardiovasc Magn Reson*. 2008;10:1-18.
- Skinner JS, Smeeth L, Kendall JM, Adams PC, Timmis A; Chest Pain Guideline Development Group. NICE guidance. Chest pain of recent onset: assessment and diagnosis of recent onset chest pain or discomfort of suspected cardiac origin. *Heart*. 2010;96:974-978.
- Schwitzer J, Nanz D, Kneifel S, et al. Assessment of myocardial perfusion in coronary artery disease by magnetic resonance: a comparison with positron emission tomography and coronary angiography. *Circulation*. 2001;103:2230-2235.
- Kanal E, Maravilla K, Rowley HA. Gadolinium contrast agents for CNS imaging: current concepts and clinical evidence. *Am J Neuroradiol*. 2014;35:2215-2226.
- Perazella M. Gadolinium-contrast toxicity in patients with kidney disease: nephrotoxicity and nephrogenic systemic fibrosis. *Curr Drug Saf*. 2008;3:67-75.
- Kanda T, Ishii K, Kawaguchi H, Kitajima K, Takenaka D. High signal intensity in the dentate nucleus and globus pallidus on unenhanced T1-weighted MR images: relationship with increasing cumulative dose of a gadolinium-based contrast material. *Radiology*. 2014;270:834-841.
- Kanda T, Nakai Y, Oba H, Toyoda K, Kitajima K, Furui S. Gadolinium deposition in the brain. *Magn Reson Imaging*. 2016;34:1346-1350.
- Detre JA, Leigh JS, Williams DS, Koretsky AP. Perfusion imaging. *Magn Reson Med*. 1992;23:37-45.
- Williams S, Detre JA, Leigh JS, Koretsky AP. Magnetic resonance imaging of perfusion using spin inversion of arterial water. *Proc Natl Acad Sci*. 1992;89:212-216.
- Haller S, Zaharchuk G, Thomas DL, Lovblad K-O, Barkhof F, Golay X. Arterial spin labeling perfusion of the brain: emerging clinical applications. *Radiology*. 2016;281:337-356.
- Hernandez-Garcia L, Lahiri A, Schollenberger J. Recent progress in ASL. *Neuroimage*. 2019;187:3-16.
- Zun Z, Wong EC, Nayak KS. Assessment of myocardial blood flow (MBF) in humans using arterial spin labeling (ASL): feasibility and noise analysis. *Magn Reson Med*. 2009;62:975-983.
- Zun Z, Varadarajan P, Pai RG, Wong EC, Nayak KS. Arterial spin labeled CMR detects clinically relevant increase in myocardial blood flow with vasodilation. *JACC Cardiovasc Imaging*. 2011;4:1253-1261.

15. Kober F, Jao T, Troalen T, Nayak KS. Myocardial arterial spin labeling. *J Cardiovasc Magn Reson*. 2016;18:1-16.
16. Buxton RB, Frank LR, Wong EC, Siewert B, Warach S, Edelman RR. A general kinetic model for quantitative perfusion imaging with arterial spin labeling. *Magn Reson Med*. 1998;40:383-396.
17. Poncelet BP, Koelling TM, Schmidt CJ, et al. Measurement of human myocardial perfusion by double-gated flow alternating inversion recovery EPI. *Magn Reson Med*. 1999;41:510-519.
18. Epstein FH, Meyer CH. Myocardial perfusion using arterial spin labeling CMR: promise and challenges. *JACC Cardiovasc Imaging*. 2011;4:1262-1264.
19. Jao T, Nayak K. Analysis of physiological noise in quantitative cardiac magnetic resonance. *PLoS One*. 2019;14:e0214566.
20. McCommis KS, Goldstein TA, Zhang H, Misselwitz B, Gropler RJ, Zheng J. Quantification of myocardial blood volume during dipyridamole and dobutamine stress: a perfusion CMR study. *J Cardiovasc Magn Reson*. 2007;9:785-792.
21. Bergmann SR, Fox KA, Rand AL, et al. Quantification of regional myocardial blood flow in vivo with H215O. *Circulation*. 1984;70:724-733.
22. Do HP, Jao TR, Nayak KS. Myocardial arterial spin labeling perfusion imaging with improved sensitivity. *J Cardiovasc Magn Reson*. 2014;16:1-6.
23. Goodwill AG, Dick GM, Kiel AM, Tune JD. Regulation of coronary blood flow. *Comprehensive Phys Ther*. 2017;7:321.
24. Heusch G. Heart rate in the pathophysiology of coronary blood flow and myocardial ischaemia: benefit from selective bradycardic agents. *Br J Pharmacol*. 2008;153:1589-1601.
25. Hermann I, Kellman P, Demirel OB, Akçakaya M, Schad LR, Weingärtner S. Free-breathing simultaneous T1, T2, and T2* quantification in the myocardium. *Magn Reson Med*. 2021;86:1226-1240.
26. Weingärtner S, Meßner NM, Budjan J, et al. Myocardial T1-mapping at 3T using saturation-recovery: reference values, precision and comparison with MOLLI. *J Cardiovasc Magn Reson*. 2017;18:1-9.
27. Do HP, Yoon AJ, Fong MW, Saremi F, Barr ML, Nayak KS. Double-gated myocardial ASL perfusion imaging is robust to heart rate variation. *Magn Reson Med*. 2017;77:1975-1980.
28. Henningsson M, Carlhäll C-J, Kihlberg J. Myocardial arterial spin labeling in systole and diastole using flow-sensitive alternating inversion recovery with parallel imaging and compressed sensing. *NMR Biomed*. 2020;34(2):e4436.
29. Aramendía-Vidaurreta V, Gordaliza PM, Vidorreta M, et al. Reduction of motion effects in myocardial arterial spin labeling. *Magn Reson Med*. 2022;87:1261-1275.
30. Ogg RJ, Kingsley RB, Taylor JS. WET, a T1- and B1-insensitive water-suppression method for in vivo localized 1H NMR spectroscopy. *J Magn Reson B*. 1994;104:1-10.
31. Weingärtner S, Akçakaya M, Basha T, et al. Combined saturation/inversion recovery sequences for improved evaluation of scar and diffuse fibrosis in patients with arrhythmia or heart rate variability. *Magn Reson Med*. 2014;71:1024-1034.
32. Messroghli DR, Radjenovic A, Kozerke S, Higgins DM, Sivananthan MU, Ridgway JP. Modified look-locker inversion recovery (MOLLI) for high-resolution T1 mapping of the heart. *Magn Reson Med*. 2004;52:141-146.
33. Wacker CM, Wiesmann F, Bock M, et al. Determination of regional blood volume and intra-extracapillary water exchange in human myocardium using Feruglose: first clinical results in patients with coronary artery disease. *Magn Reson Med*. 2002;47:1013-1016.
34. Nickander J, Themudo R, Thalén S, et al. The relative contributions of myocardial perfusion, blood volume and extracellular volume to native T1 and native T2 at rest and during adenosine stress in normal physiology. *J Cardiovasc Magn Reson*. 2019;21:1-10.
35. Mizukoshi K, Takeuchi M, Nagata Y, et al. Normal values of left ventricular mass index assessed by transthoracic three-dimensional echocardiography. *J Am Soc Echocardiogr*. 2016;29:51-61.
36. Tao Q, Tol P, Berendsen FF, Paiman EHM, Lamb HJ, Geest RJ. Robust motion correction for myocardial T1 and extracellular volume mapping by principle component analysis-based groupwise image registration. *J Magn Reson Imaging*. 2018;47:1397-1405.
37. Cerqueira MD, Weissman NJ, Dilsizian V, et al. Standardized myocardial segmentation and nomenclature for tomographic imaging of the heart: a statement for healthcare professionals from the Cardiac Imaging Committee of the Council on Clinical Cardiology of the American Heart Association. *Circulation*. 2002;105:539-542.
38. Weingärtner S, Desmond KL, Obuchowski NA, et al. Development, validation, qualification, and dissemination of quantitative MR methods: overview and recommendations by the ISMRM quantitative MR study group. *Magn Reson Med*. 2022;87:1184-1206.
39. Qiu M, Paul Maguire R, Arora J, et al. Arterial transit time effects in pulsed arterial spin labeling CBF mapping: insight from a PET and MR study in normal human subjects. *Magn Reson Med*. 2010;63:374-384.
40. Wong EC, Buxton RB, Frank LR. Quantitative imaging of perfusion using a single subtraction (QUIPSS and QUIPSS II). *Magn Reson Med*. 1998;39:702-708.
41. Landes V, Javed A, Jao T, Qin Q, Nayak K. Improved velocity-selective labeling pulses for myocardial ASL. *Magn Reson Med*. 2020;84:1909-1918.
42. Jao TR, Nayak KS. Demonstration of velocity selective myocardial arterial spin labeling perfusion imaging in humans. *Magn Reson Med*. 2018;80:272-278.
43. Wang DJJ, Bi X, Avants BB, Meng T, Zuehlsdorff S, Detre JA. Estimation of perfusion and arterial transit time in myocardium using free-breathing myocardial arterial spin labeling with navigator-echo. *Magn Reson Med*. 2010;64:1289-1295.
44. Troalen T, Capron T, Cozzone PJ, Bernard M, Kober F. Cine-ASL: a steady-pulsed arterial spin labeling method for myocardial perfusion mapping in mice. Part I. experimental study. *Magn Reson Med*. 2013;70:1389-1398.
45. Lee NG, Javed A, Jao TR, Nayak KS. Numerical approximation to the general kinetic model for ASL quantification. *Magn Reson Med*. 2020;84:2846-2857.
46. Weingärtner S, Zimmer F, Metzger GJ, Uğurbil K, Moortele P-F, Akçakaya M. Motion-robust cardiac mapping at 3T using interleaved Bloch-Siegert shifts. *Magn Reson Med*. 2017;78:670-677.
47. Messroghli DR, Moon JC, Ferreira VM, et al. Clinical recommendations for cardiovascular magnetic resonance mapping of T1, T2, T2* and extracellular volume: a consensus statement by the Society for Cardiovascular Magnetic Resonance (SCMR) endorsed by the European Association for Cardiovascular Imaging (EACVI). *J Cardiovasc Magn Reson*. 2017;19:1-24.

48. Chareonthaitawee P, Kaufmann PA, Rimoldi O, Camici PG. Heterogeneity of resting and hyperemic myocardial blood flow in healthy humans. *Cardiovasc Res.* 2001;50:151-161.
49. Kellman P, Hansen MS, Nielles-Vallespin S, et al. Myocardial perfusion cardiovascular magnetic resonance: optimized dual sequence and reconstruction for quantification. *J Cardiovasc Magn Reson.* 2017;19:1-14.
50. Brown LAE, Gulsin GS, Onciul SC, et al. Sex-and age-specific normal values for automated quantitative pixel-wise myocardial perfusion cardiovascular magnetic resonance. *Eur Heart J Cardiovasc Imaging.* 2023;24:426-434.
51. Aramendía-Vidaurreta V, García-Osés A, Vidorreta M, Bastarrika G, Fernández-Seara MA. Optimal repetition time for free breathing myocardial arterial spin labeling. *NMR Biomed.* 2019;32:e4077.
52. Knott KD, Camaioni C, Ramasamy A, et al. Quantitative myocardial perfusion in coronary artery disease: a perfusion mapping study. *J Magn Reson Imaging.* 2019;50:756-762.
53. Gould KL, Johnson NP, Bateman TM, et al. Anatomic versus physiologic assessment of coronary artery disease: role of coronary flow reserve, fractional flow reserve, and positron emission tomography imaging in revascularization decision-making. *J Am Coll Cardiol.* 2013;62:1639-1653.
54. Ferreira PF, Gatehouse PD, Mohiaddin RH, Firmin DN. Cardiovascular magnetic resonance artefacts. *J Cardiovasc Magn Reson.* 2013;15:1-39.
55. Staffeld HF, Mertens HM, Gleichmann U. Influence of dynamic exercise and training on systolic time intervals in normals and patients with coronary heart disease (author's transl). *Zeitschrift Fur Kardiol.* 1978;67:305-316.
56. Schmid S, Ghariq E, Teeuwisse WM, Webb A, Osch MJ. Acceleration-selective arterial spin labeling. *Magn Reson Med.* 2014;71:191-199.
57. Zhang H, Shea SM, Park V, et al. Accurate myocardial T1 measurements: toward quantification of myocardial blood flow with arterial spin labeling. *Magn Reson Med.* 2005;53:1135-1142.
58. Miyazaki M, Zhou X, Hoshino T, Yokoyama K, Ishimura R, Nitatori T. Non-contrast myocardial perfusion using a novel 4D magnetic resonance arterial spin labeling technique: initial experience. *Microvasc Res.* 2015;98:94-101.
59. Heidenreich JF, Weng AM, Donhauser J, et al. T1-and ECV-mapping in clinical routine at 3 T: differences between MOLLI, ShMOLLI and SASHA. *BMC Med Imaging.* 2019;19:1-9.
60. Chow K, Flewitt JA, Green JD, Pagano JJ, Friedrich MG, Thompson RB. Saturation recovery single-shot acquisition (SASHA) for myocardial T1 mapping. *Magn Reson Med.* 2014;71:2082-2095.
61. Cunningham CH, Pauly JM, Nayak KS. Saturated double-angle method for rapid B1+ mapping. *Magn Reson Med.* 2006;55:1326-1333.
62. Bruyne B, Bartunek J, Sys SU, Pijls NHJ, Heyndrickx GR, Wijns W. Simultaneous coronary pressure and flow velocity measurements in humans: feasibility, reproducibility, and hemodynamic dependence of coronary flow velocity reserve, hyperemic flow versus pressure slope index, and fractional flow reserve. *Circulation.* 1996;94:1842-1849.
63. Scheffler K. On the transient phase of balanced SSFP sequences. *Magn Reson Med.* 2003;49:781-783.

SUPPORTING INFORMATION

Additional supporting information may be found in the online version of the article at the publisher's website.

Figure S1. Coefficient of variation of simulated myoASL-MBF as a function of heart rate variability.

Figure S2. Simulated and phantom myoASL-MBF as a function of the control-tag delay.

Figure S3. Phantom myoASLMBF as a function of heart rate and blood T1.

Figure S4. Simulated myoASLMBF deviation as a function of acquisition flip angle and matrix size.

Figure S5. Simulated myoASLMBF as a function of blood T1 and T2 relaxation times.

Figure S6. Simulated myoASLMBF deviation as a function of blood T1 error.

Figure S7. Simulated myoASLMBF as a function of heart rate and blood T1.

How to cite this article: Božić-Iven M, Rapacchi S, Tao Q, et al. Improved reproducibility for myocardial ASL: Impact of physiological and acquisition parameters. *Magn Reson Med.* 2023;1-15. doi: 10.1002/mrm.29834

APPENDIX A. SIGNAL EQUATIONS FOR BSSFP AND SPGRE READOUT

A.1 bSSFP readout

The MMF for a bSSFP readout can be expressed via the transient state magnetization as described by Scheffler.⁶³ For a readout with flip angle (FA) α and an $\frac{\alpha}{2}$ -preparation pulse, the magnetization vector after the k -th RF pulse can be given as:⁶³

$$\mathbf{M}(k) = \left(\sin \left(\frac{\alpha}{2} \right) \mathbf{M}_0 - \mathbf{M}_{ss} \right) \lambda_1^k + \mathbf{M}_{ss}, \quad (\text{A1})$$

with initial magnetization \mathbf{M}_0 , steady-state magnetization $\mathbf{M}_{ss} = \rho \frac{\sqrt{E_2(1-E_1)} \sin(\alpha)}{1-(E_1-E_2) \cos(\alpha) - E_1 E_2}$, proton density ρ , coefficients $E_{1/2} = e^{-TR/T_{1/2}}$, and the eigenvalue λ_1 :

$$\begin{aligned} \lambda_1 &= \cos(\alpha)(E_1 - E_2) + \sqrt{\cos^2(\alpha)(E_1 - E_2)^2 + 4E_1 E_2} \\ &\approx E_1 \cos^2 \left(\frac{\alpha}{2} \right) + E_2 \sin^2 \left(\frac{\alpha}{2} \right). \end{aligned} \quad (\text{A2})$$

With $x = M_z(t_0)$ the MMF becomes:

$$f_{\text{MMF}}^{\text{bSSFP}}(x) = \sin \left(\frac{\alpha}{2} \right) \lambda_1^k x + (1 - \lambda_1^k) M_{ss}. \quad (\text{A3})$$

A.2 spGRE readout

Similarly, the MMF for a spGRE readout can be derived based on the Bloch equations. After a first RF pulse with FA α at t_0 and a second after a repetition time TR, the longitudinal magnetization $M_z(t_0 + \text{TR})$ is given by

$$M_z(t_0 + \text{TR}) = \cos^2(\alpha)E_1M_z(t_0) + \cos(\alpha)(1 - E_1)M_{z,\text{eq}}, \quad (\text{A4})$$

with initial magnetization $M_z(t_0)$ and equilibrium magnetization $M_{z,\text{eq}}$. After k RF pulses, the longitudinal magnetization yields

$$M_z(k) = \cos^k(\alpha)E_1^{-(k-1)}M_z(t_0) + \left(\sum_{i=0}^{k-2} (\cos(\alpha)E_1)^{-i} \right) \cos(\alpha)(1 - E_1), \quad (\text{A5})$$

and the MMF for spGRE can be given as

$$f_{\text{MMF}}^{\text{spGRE}}(x) = \cos^k(\alpha)E_1^{-(k-1)}x + \frac{1 - (\cos(\alpha)E_1)^{n-1}}{1 - \cos(\alpha)E_1}(1 - E_1)\cos(\alpha)\rho M_{z,\text{eq}}. \quad (\text{A6})$$

APPENDIX B. IMAGING SIGNAL FOR BASELINE, CONTROL AND TAG IMAGE IN FAIR-MYOASL

In both, control and tag images, the myocardium is inverted in the imaging slice and recovers with $T_{1,M}$ during the time TI preceding the imaging readout. Using Equation (2), the myocardial signal contribution can thus be expressed as

$$I_M = V_M(A_Mx_M^- + B_M), \quad (\text{B1})$$

where $x_M^- = 1 - e^{-TI/T_{1,M}}$.

The blood signal, however, differs between the two settings. After the slice-selective inversion in the control image, noninverted blood flows into the imaging slice with in-flow rate f_{in} giving rise to the signal contribution

$$I_{C,B}^+ = V_B f_{\text{in}}(A_Bx_B^+ + B_B), \quad (\text{B2})$$

with $x_B^+ = 1$. At the same time outflow of the initially inverted blood occurs with the same rate f_{in} , such that

the remaining noninverted blood contributes to the signal with

$$I_{C,B}^- = V_B(1 - f_{\text{in}})(A_Bx_B^- + B_B), \quad (\text{B3})$$

where $x_B^- = 1 - e^{-TI/T_{1,B}}$. Combining Equations (B2) and (B3) the full contribution of blood signal to the control image yields:

$$I_{C,B} = V_B(f_{\text{in}}(A_Bx_B^+ + B_B) + (1 - f_{\text{in}})(A_Bx_B^- + B_B)). \quad (\text{B4})$$

In tag images, the in-flowing blood is also inverted due to the non-selective inversion, and can be expressed as

$$I_{T,B} = V_B(A_Bx_B^- + B_B). \quad (\text{B5})$$

Finally, in the case of the baseline image, neither myocardium nor blood is inverted ($x_M^+ = x_B^+ = 1$):

$$\begin{aligned} I_{BL,B} &= V_B(A_Bx_B^+ + B_B) \\ I_{M,BL} &= V_M(A_Mx_M^+ + B_M). \end{aligned} \quad (\text{B6})$$

Combining the signal contributions from Equations (B1)–(B6), yields the following signal equations for the control (I_C), tag (I_T), and baseline signal (I_{BL}) in FAIR-myoASL:

$$\begin{aligned} I_C &= I_M + I_{C,B} = \\ &= V_M(A_Mx_M^- + B_M) \\ &+ V_B(f_{\text{in}}(A_Bx_B^+ + B_B) + (1 - f_{\text{in}})(A_Bx_B^- + B_B)), \end{aligned} \quad (\text{B7})$$

$$\begin{aligned} I_T &= I_M + I_{T,B} = \\ &= V_M(A_Mx_M^- + B_M) + V_B(A_Bx_B^- + B_B), \end{aligned} \quad (\text{B8})$$

$$\begin{aligned} I_{BL} &= I_{M,BL} + I_{BL,B} = \\ &= V_M(A_Mx_M^+ + B_M) + V_B(A_Bx_B^+ + B_B). \end{aligned} \quad (\text{B9})$$

Subtracting this saturation-baseline from the original baseline image yields

$$\begin{aligned} I_{BL} - I_{BL,\text{Sat}} &= V_M(A_Mx_M^+ + B_M) + V_B(A_Bx_B^+ + B_B) \\ &- (V_M(A_M \cdot 0 + B_M) + V_B(A_B \cdot 0 + B_B)) = \\ &= V_M A_M x_M^+ + V_B A_B x_B^+. \end{aligned} \quad (\text{B10})$$